

FINAL REPORT

Project Title: Computational Modeling and Simulation of Film-Condensation

Project Number: AOARD -14080

Investigators: Dr. Atul Sharma and Dr. Amit Agrawal, IIT Bombay, INDIA

Started on: 29/9/11

Ended on: 29/9/12

TECHNICAL MILESTONES PROPOSED AND THE PRESENT STATUS

1. Development of Computational methodology for simulation of film-condensation: COMPLETED
 2. Development and testing of a level set method based code for film-condensation in 2D Cartesian coordinate: COMPLETED
 3. Develop proper computational set-up for the present numerical simulation: COMPLETED
 4. A detailed analysis of the results obtained by a parametric study of the film-condensation in a plane channel: COMPLETED
 5. An attempt will be made to develop another code in 3D cylindrical coordinate for the film-condensation in a pipe: IN-PROGRESS
-

SUMMARY

The researchers in AFRL are trying to model and analyze flow in a condenser of a vapor-compression refrigeration system used for thermal management of electronic components in aircrafts. The present work is an effort in that direction to model, simulate and analyze film condensation.

A novel dual-grid level set method based modeling and simulation of film-condensation is discussed here. An in-house code is used for the analysis of two different film condensation problems: first, on the underside of a horizontal plate and second, in a plane channel. The first study is done at various degree of sub-cooling of the plate, with R-123 and n-pentane as the working fluid; and various unsteady flow regimes and its effect on heat transfer is reported. The second study is done analytically for fully-developed and numerically for developing flow in a channel, with an excellent agreement between the two results in the fully developed region. The simulations are done for four different cases, consisting of various standard thermal boundary conditions on the channel wall. The numerical results obtained for the developing flow are consistent with the physical-model and operating-conditions proposed in the present work.

Although the present work is fundamental in nature, the modeling and simulation strategy presented here can be extended for to model and analyze flow in a condenser for better design and integration in thermal-management systems in many aircrafts.

Report Documentation Page

*Form Approved
OMB No. 0704-0188*

Public reporting burden for the collection of information is estimated to average 1 hour per response, including the time for reviewing instructions, searching existing data sources, gathering and maintaining the data needed, and completing and reviewing the collection of information. Send comments regarding this burden estimate or any other aspect of this collection of information, including suggestions for reducing this burden, to Washington Headquarters Services, Directorate for Information Operations and Reports, 1215 Jefferson Davis Highway, Suite 1204, Arlington VA 22202-4302. Respondents should be aware that notwithstanding any other provision of law, no person shall be subject to a penalty for failing to comply with a collection of information if it does not display a currently valid OMB control number.

1. REPORT DATE 18 JAN 2013		2. REPORT TYPE Final		3. DATES COVERED 29-09-2011 to 29-09-2012	
4. TITLE AND SUBTITLE Computational Modeling and Simulation of Film-Condensation				5a. CONTRACT NUMBER FA23861114080	
				5b. GRANT NUMBER	
				5c. PROGRAM ELEMENT NUMBER	
6. AUTHOR(S) Atul Sharma				5d. PROJECT NUMBER	
				5e. TASK NUMBER	
				5f. WORK UNIT NUMBER	
7. PERFORMING ORGANIZATION NAME(S) AND ADDRESS(ES) Indian Institute of Technology- Bombay, IIT Bombay, Powai, Mumbai 400076, India, IN, 400076				8. PERFORMING ORGANIZATION REPORT NUMBER N/A	
9. SPONSORING/MONITORING AGENCY NAME(S) AND ADDRESS(ES) AOARD, UNIT 45002, APO, AP, 96338-5002				10. SPONSOR/MONITOR'S ACRONYM(S) AOARD	
				11. SPONSOR/MONITOR'S REPORT NUMBER(S) AOARD-114080	
12. DISTRIBUTION/AVAILABILITY STATEMENT Approved for public release; distribution unlimited					
13. SUPPLEMENTARY NOTES					
14. ABSTRACT This report describes an investigation of modeling and analysis of two-phase flow in the condenser of a vapor-compression refrigeration system. The approach used a novel in-house code for the analysis of two different film condensation problems: a) underside of a horizontal plate, b) in a plane channel. In the first study, the effect on heat transfer was determined at various degrees of sub-cooling of the plate and at various unsteady flow regimes using R-123 and n-pentane as working fluids. The second study was done analytically for fully-developed and numerically for developing flow in a channel; excellent agreement between the two results was observed in the fully developed region. Simulations were done for four different cases, consisting of various standard thermal boundary conditions on the channel wall. Numerical results obtained for the developing flow are consistent with the physical-model and operating-conditions proposed in the present work. The findings from this fundamental modeling and simulation study can be extended to model and analyze condenser flow for better design and integration in thermal-management systems found in aircraft.					
15. SUBJECT TERMS Heat & Mass Transfer, Condensation modeling, Condensation modeling, Level set method, Thoretical and modeling techniques					
16. SECURITY CLASSIFICATION OF:			17. LIMITATION OF ABSTRACT	18. NUMBER OF PAGES	19a. NAME OF RESPONSIBLE PERSON
a. REPORT	b. ABSTRACT	c. THIS PAGE			
unclassified	unclassified	unclassified	Same as Report (SAR)	18	

TECHNICAL REPORT

The report consists of three different sections: first, computational-methodology; second, code-validation; and third, computational fluid dynamics study on film condensation. The study is done on two different problems, film condensation on the underside of a horizontal plate and in a plane channel.

1. Computational Methodology

Level-set method is an Eulerian technique to capture the two-phase interface (Gada and Sharma, 2009). The level-set function (ϕ) is defined as a signed normal distance function measured from the interface such that $\phi = 0$ on the interface; $\phi > 0$ in the heavier fluid, phase 1 (liquid phase); $\phi < 0$ in the lighter fluid, phase 2 (vapor phase).

Navier-Stokes equations are discretized by finite volume and level set equations by finite difference method. A Semi-Explicit pressure projection method is used to solve the NS equations on a staggered grid. Energy equation is solved using sharp-interface method. Temporal term is discretized using Euler explicit method for NS equation and 3rd order Runge-Kutta method for LS advection equation. Advection term is discretized by 2nd order TVD LINLIN scheme for momentum/energy equation and 5th order WENO scheme for LS advection equation. Diffusion term is discretized by 2nd order central-difference scheme.

A novel dual-grid level-set method (Gada and Sharma, 2011) is adopted in the present study. It utilizes a double refined grid to discretize the level-set function and the temperature, when compared to the pressure and velocity field variables. Furthermore, a diffused interface formulation is used to solve the flow field, while a sharp interface treatment is applied for solving the energy equation (Gada, 2012). This treatment is validated on a Stefan problem, discussed in the next section.

2. Code-Validation

Although the in-house code is validated on Stefan problem here, its validation for film-condensation on the underside of a horizontal plate and in a plane channel is discussed in Section 3 below.

Stefan problem represents a phase change process progressing in one-dimension over a semi-infinite domain (Alexiades and Solomon, 1993), as shown in Fig. 1. Initially, the entire domain is filled with saturated vapor. At time $\tau = 0$, the left wall is suddenly sub-cooled and maintained at $T_w < T_{sat}$. This triggers a condensation process resulting in the formation of a liquid layer between the wall and the vapor. Thereafter, the liquid-vapor interface thus formed keeps moving away from the wall due to condensation occurring at the interface, where the vapor continually loses its latent heat to the liquid side. At the same time, a temperature gradient builds up on the liquid side due to heat diffusion from the interface to the wall through the liquid layer.

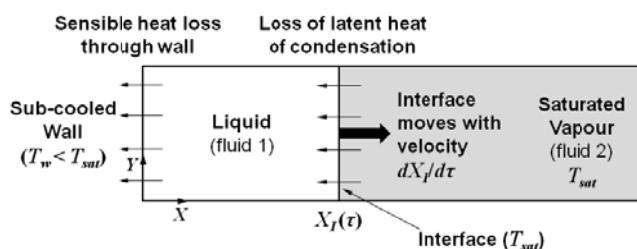


Figure 1: Schematic of 1D Stefan problem

This phenomenon is governed by an unsteady one-dimensional diffusion equation (which is solved in the liquid phase only). In the non-dimensional form, the governing equation is given as

$$\frac{\partial \theta}{\partial \tau} = \frac{\partial^2 \theta}{\partial X^2} \text{ for } 0 \leq X \leq X_I(\tau); \tau \geq 0 \quad (1)$$

Here, X_I is the instantaneous location of the interface; $\theta = (T - T_{sat})/(T_{sat} - T_w)$ is the non-dimensional temperature, $X = x/L_c$ is the traverse location, $\tau = t\alpha_1/L_c^2$ is the non-dimensional time; L_c being the characteristic length scale, which is taken equal to the domain height for this problem.

The initial and boundary conditions are given as

$$\text{Initial: } X_I(0) = 0 \text{ and } \theta(X, 0) = 0 \quad (2)$$

$$\text{Left boundary: } \theta(0, \tau) = -1 \text{ for } \tau > 0 \quad (3)$$

$$\text{Right Boundary: } \theta(X_I, \tau) = 0 \text{ for } \tau > 0 \quad (4)$$

The instantaneous location of the right boundary, $X_I(\tau)$, can be found by using Eq. (5); which is obtained by applying energy balance at the interface. Here, the vapor to liquid mass conversion rate at the interface is balanced by the heat diffusing into the liquid side, while neglecting the heat diffusion into the vapor side.

Here, $St_1 = c_{p1}(T_{sat} - T_w)/h_{12}$

$$\frac{dX_I}{d\tau} = -St_1 \left. \frac{d\theta}{dX} \right|_{X=X_I} \text{ for } \tau > 0 \quad (5)$$

The results obtained with n-pentane as the working fluid (properties given in Table 1), on a non-dimensional domain size of 100×10 , with a grid size of 100×10 and $L_c = 0.0001\text{m}$, is compared with the analytical results (Alexiades and Solomon, 1993) and an excellent agreement is shown in Fig. 2.

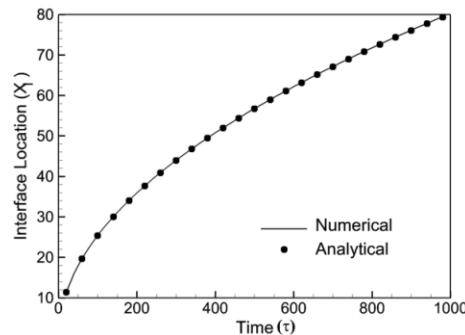


Figure 2: Comparison of interface evolution obtained numerically and analytically for the Stefan problem

3. Computational Fluid Dynamics Study on Film Condensation

For the first time, condensation studies are done from our in-house code (Gada and Sharma, 2011), developed for multiphase flow. Two different problems are simulated and analyzed, discussed below in separate subsections.

3.1. CFD Analysis of Film Condensation on the underside of a Horizontal Plate

It is concluded from a literature review that very few studies have been performed for condensation on a downward facing plate, especially numerically. The present study aims at

understanding the effect of increasing heat removal rates on the nature of condensate flow. With increasing condensate flow rates, the flow modes are expected to undergo transitions; as suggested by studies on falling films (Dhir and Taghavi-Tafreshi, 1981; Hu and Jacobi, 1996). The effect of such a transition on Nusselt number is not found in literature. Therefore, the aim of the present study is to elucidate the transition of condensate flow regimes and their effects with increasing degree of sub-cooling.

3.1.1. Physical Description of the Problem

The schematic of the domain for the problem under consideration is shown in Fig. 3. A flat surface, cooled from above, forms the top boundary of the domain. Saturated vapors lose heat to this sub-cooled surface; thereby, forming a condensate film which wets the underside of the top boundary. The liquid film being unstable, under the forces of gravity and surface tension, grows into droplets which eventually pinch-off and fall into the bulk vapor. This can be attributed to a “Taylor instability” that occurs at the interface whenever a heavier fluid sits on top of a lighter one. This instability grows in the form of waves. The wavelength at which such disturbances grow most rapidly is called the “most dangerous wavelength” (λ_d ; given by Eq. (6)) (Bellman and Pennington, 1954; Sharifi and Esmaceli, 2009). Because of their rapid growth rate, disturbances with the most dangerous wavelength are expected to occur most often in practice.

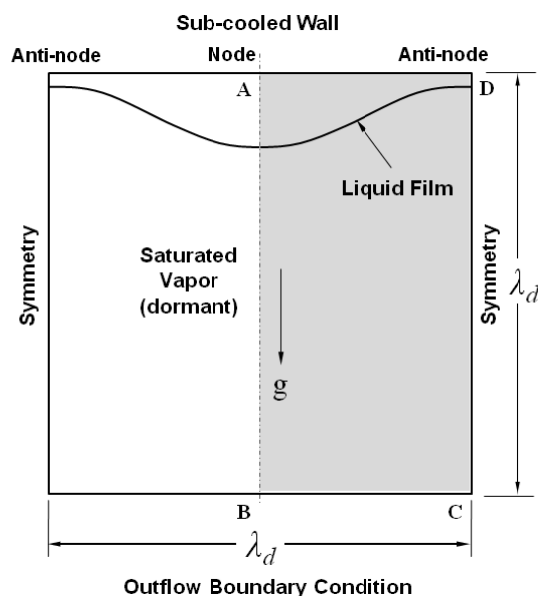


Figure 3: Computational domain for condensation on the underside of a horizontal plate

3.1.2. Numerical Details

A domain of size $\lambda_d \times \lambda_d$ is sufficient to capture the spatially periodic phenomenon of droplet-jet formation/release during condensation. Similar domain definitions have proven to suffice in the past studies on film boiling (Welch and Wilson, 2000; Tomar et al., 2005) and condensation (Sharifi and Esmaceli, 2009), where the flow is governed by the Taylor instability. Furthermore, due to its symmetry along the centerline of the domain, a computational domain ABCD (shown by the shaded region in Fig. 3) of size $0.5\lambda_d \times \lambda_d$ suffices for the present analysis, with symmetry boundary conditions applied on its left and right boundaries.

Two refrigerants are selected for the present study, namely R-123 and n-pentane. Table 1 shows their properties and working conditions. A grid size of 100×200 and 125×250 are found sufficient to give grid independent results for n-pentane and R-123, respectively. The liquid film is perturbed initially using the curve given by Eq. (7) below.

$$\lambda_d = 2\pi \sqrt{\frac{3\sigma}{g(\rho_1 - \rho_2)}} \quad (6)$$

$$y = \lambda_d \left[\frac{1}{40} - \frac{1}{64} \cos\left(\frac{2\pi x}{\lambda_d}\right) \right] \quad (7)$$

Table 1: Properties of working fluids (in SI units)

	n-pentane		R-123	
	Liquid	Vapor	Liquid	Vapor
T_{sat}	468.3		455.8	
P_{sat}	3.3×10^6		3.6×10^6	
ρ	296.53	173.22	686.39	414.29
$\mu \times 10^5$	3.27	1.88	5.52	3.13
k	0.05599	0.04555	0.03915	0.03227
$c_p \times 10^{-4}$	2.39	3.52	1.47	1.91
σ	3.82×10^{-5}		3.07×10^{-5}	
h_{fg}	5.72×10^4		2.54×10^4	

The boundary conditions are shown qualitatively in Fig. 3. The sub-cooled wall is considered to be cooled uniformly; namely having a constant degree of sub-cooling, $\Delta T_{sat} = T_{sat} - T_w = \text{constant}$. The boundary conditions on the left and right boundaries are given by Eq. (8) and those on the bottom by Eq. (9). Top wall boundary conditions are summarized by Eq. (10) below. The details on the equation and non-dimensionalization can be found in Gada and Sharma (2009). Here, the characteristic temperature scale is taken as ΔT_{sat} .

$$\frac{\partial U}{\partial X} = 0; V = 0; \frac{\partial P}{\partial X} = 0; \frac{\partial \phi}{\partial X} = 0; \frac{\partial \theta}{\partial X} = 0 \quad (8)$$

$$\frac{\partial U}{\partial Y} = 0; \frac{\partial V}{\partial Y} = 0; P = 0; \frac{\partial \phi}{\partial Y} = 0; \frac{\partial \theta}{\partial Y} = 0 \quad (9)$$

$$U = 0; V = 0; \frac{\partial P}{\partial Y} = 0; \frac{\partial \phi}{\partial Y} = 0; \theta = -1 \quad (10)$$

3.1.3. Results and Discussions

Simulations are done for two different working fluids: R-123 and n-pentane (thermophysical properties and saturation condition given in Table 1 above), at various degree of sub-cooling of the horizontal plate varying from 10 to 16 K. Both the working fluids indicate a transition in the condensate flow regime from a droplet flow mode to a jet flow mode, over a very narrow range of degree of sub-cooling.

Four flow regimes were clearly identified with increasing degree of wall sub-cooling, through the droplet-jet transition:

- I. DRIPPING MODE: Periodic single droplet release at node and anti-node ($10K$).
- II. DRIPPING MODE: Periodic two droplet release at node and one at anti-node ($12K$).
- III. DRIP-JET MODE: Jetting mode at node and periodic two droplet release at anti-node ($13K$).
- IV. JETTING MODE: Steady jet flow mode ($16K$).

Transition during condensation of n-pentane

The transition regimes obtained for this case are shown in Fig. 4(a)-(d). Here, a series of snapshots are shown to depict the progression of flow over two cycles of droplet release, one at the node and other at the anti-node, with increasing values of ΔT_{sat} . Further, these can also be correlated with the instantaneous surface averaged Nusselt numbers ($Nu_{avg}(\tau)$), plotted in Fig. 4(e).

In regime I, Fig. 4(a1-a5) shows periodically alternating single droplet release at the node and anti-nodes. Whereas, in regime II, Fig. 4(b1-b5) shows that the number of droplets released are two at the node and one at the anti-node. Therefore, the periodic variation of $Nu_{avg}(\tau)$ for the release at node and anti-node are same in regime I (Fig. 4(e1)) but not in regime II (Fig. 4(e2)). Regime III experiences increased condensate flow rates, which results in the formation of a continuous jet at the node; while the condensate continues to flow in the form of drops at the anti-node location. It is interesting to note that each periodic droplet release cycle at the anti-node consists of two droplets. Therefore, this regime also attains a periodic variation of $Nu_{avg}(\tau)$; with an increase in its values compared to the previous regimes, as seen in Fig. 4(e3).

Finally, the flow transits to the steady jet flow mode in regime IV, where the droplet release at the anti-node continues initially in the form of tip-streaming (*i.e.* drops are continuously released with the breakup length increasing gradually), which finally leads to a steady flowing jet formation. Therefore, the corresponding $Nu_{avg}(\tau)$ reaches a steady value. Such flow regimes with increasing mass flow rates, have also been observed experimentally for falling films over horizontal tubes, as shown in Fig. 5.

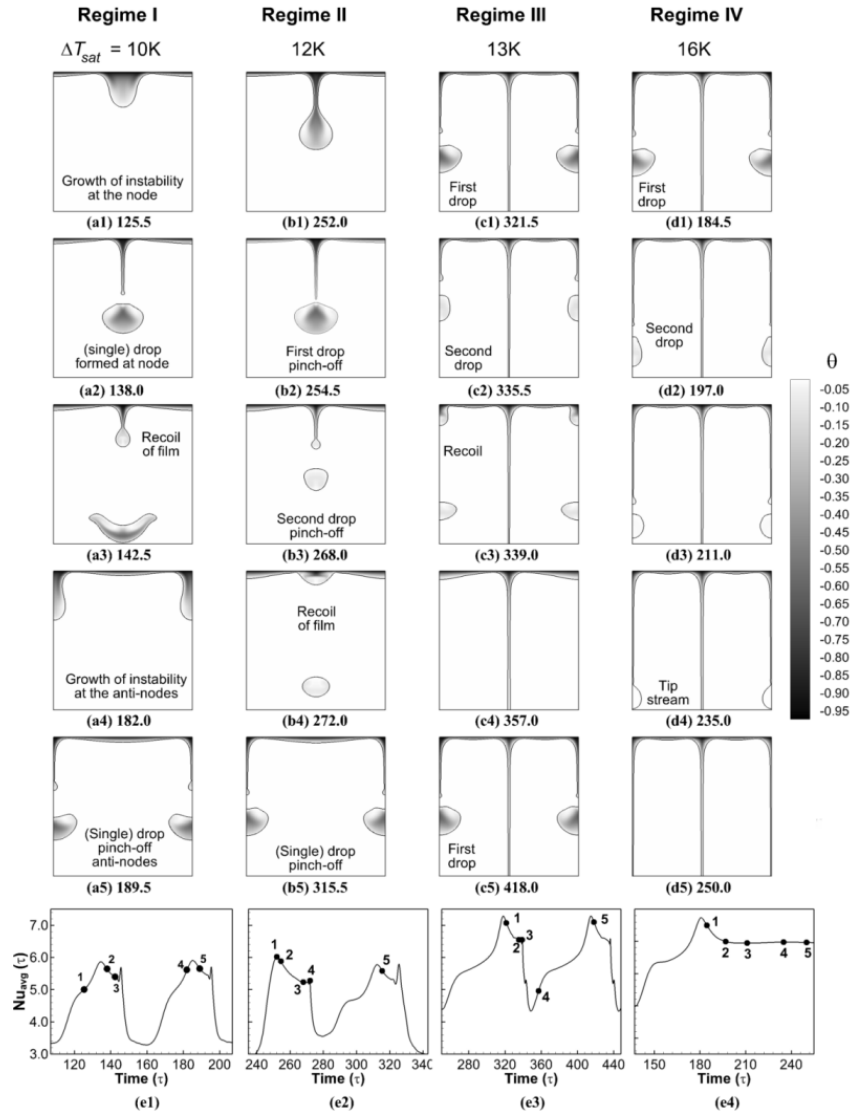


Figure 4: Transition phases observed during condensation of n-pentane, at various degree of sub cooling.

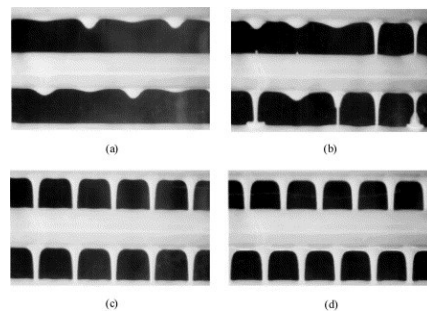


Figure 5: Flow modes obtained experimentally during drop-jet transition, with ethylene glycol flowing between horizontal tube banks (a) droplet (b) droplet-jet (c) in-line jet (d) staggered jet (Hu and Jacobi, 1996)

Transition during condensation of R-123

The drop-jet transition with R-123 followed trends similar to those obtained with n-pentane. However, some differences were seen in the flow patterns obtained in regime II and III. In regime II, a clear distinction from regime I was not obtained, as the flow was oscillating between single and double droplet releases at the node itself. Nevertheless, it must be noted that the transition for R-123 happens over very small temperature ranges (see Fig. 7(b)). Therefore, it is likely that regime II lies within a still smaller range; which is not captured while increasing ΔT_{sat} in steps. Further, regime III was characterized by a continuous jet at the node and periodic release of a single droplet at the anti-node (whereas two droplet releases at the anti-node were seen for n-pentane). This can be attributed to the lower condensate flow rates obtained in the case of R-123. This is evidenced from the local plots of average film velocities U_{avg} and film thickness A_{film} , as shown in Fig. 6. It is seen that $U_{avg,x}$ is higher for n-pentane as compared to n-pentane, while the flow areas remain nearly identical.

Surface averaged Nusselt number

Variation of the time and wall averaged Nusselt number (Nu_{AVG}) with increasing ΔT_{sat} is plotted in Fig. 7; and also compared with a heat transfer correlation proposed by Gerstmann and Griffith, 1967. Further, the progression of the flow modes is also identified in Fig. 7, with the grey areas denoting erratic flows during transition between various regimes. Fig. 7 shows good agreement between the present and published results in regime I and II (this is expected since the correlation has been proposed using data obtained in the droplet flow mode), it disagrees by as much as 40-50% in regime III and IV.

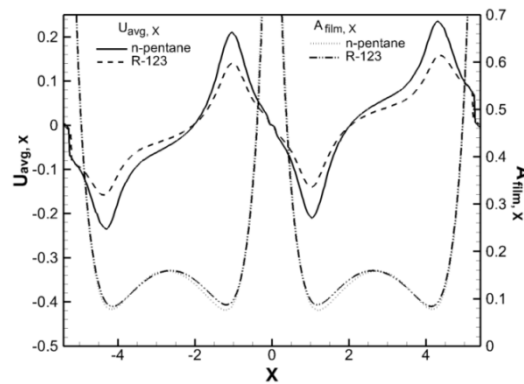


Figure 6: Local variation of U_{avg} and A_{film} obtained on the sub-cooled wall with n-pentane (R-123) at $\Delta T_{sat} = 13K$ (5K) and $\tau = 318.5$ (377)

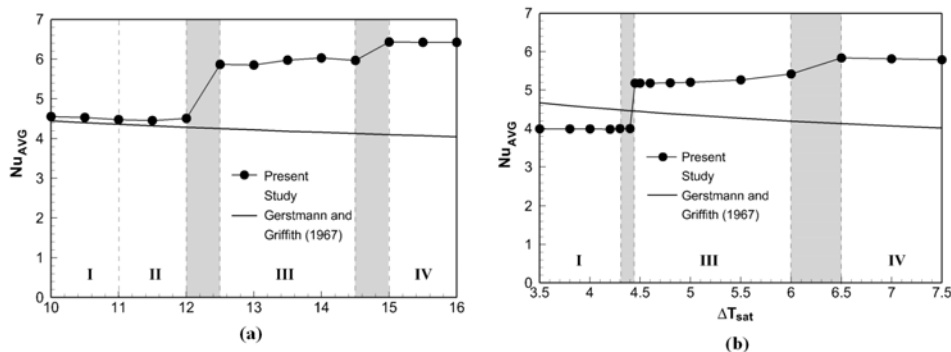


Figure 7: Behavior of time and wall averaged Nusselt number for (a) n-pentane and (b) R-123

Factors influencing the behavior of local and surface averaged Nusselt number

In any of the flow regimes, the heat transfer from the top plate will depend on the temperature gradient existing across the condensate film wetting the wall, the film thickness, the interfacial area of the film (where phase change occurs) and the average velocity in the condensate film. The local variations of some of these variables over the top wall are shown in Fig. 8.

Figure 8 is drawn at time instants when $Nu_{avg}(\tau)$ reaches the peak value in its cyclic variations plotted in Fig.4(e). Here, Nu_X is the local Nusselt number evaluated on the sub-cooled (top) wall; $U_{avg,X}$ is the average u -velocity of the condensate film at any location X ; $A_{film,X}$ is the condensate film thickness at any location X (therefore, $A_{film,X}$ can be considered to be a representation of the interface shape near the wall). It can be seen that the point of minimum film thickness coincides with the point of maximum Nu_X . Therefore, heat diffusion through the film plays a dominant role in controlling the value of Nu_X .

Further, for both the flow modes, regime I ($\Delta T_{sat} = 10K$) and regime III ($\Delta T_{sat} = 13K$), the peak values of Nu_X are nearly identical. However, four peaks per wavelength in regime III are responsible for a higher Nu_{AVG} compared to regime I. Further, the peak values of $U_{avg,X}$ occur slightly downstream of the point of maximum heat transfer coefficient.

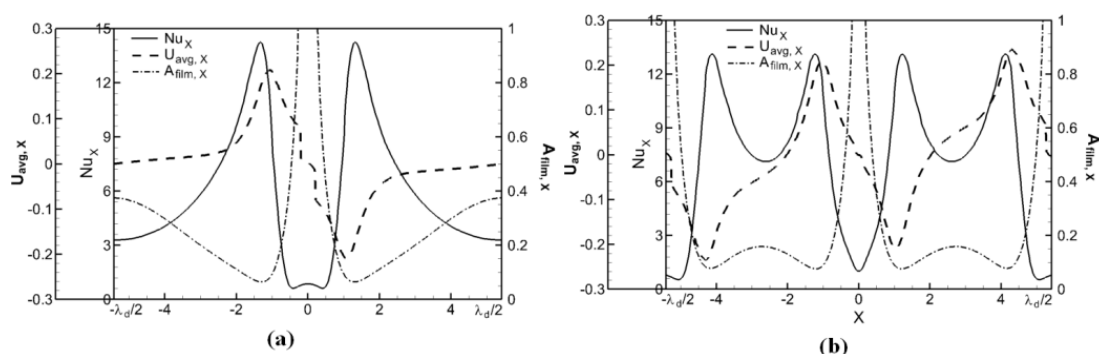


Figure 8: Local variation of U_{avg} , Nu , A_{film} on the sub-cooled wall with n-pentane (a) $\Delta T_{sat} = 10K$ at $\tau = 135.0$ (b) $\Delta T_{sat} = 13K$ at $\tau = 318.5$

3.1.4. Conclusion

Direct numerical simulations for condensation on the underside of a uniformly cooled surface were performed using a dual-grid level-set methodology. R-123 and n-pentane were considered as the working fluids. Results show that the flow transits from a drop flow mode to a steady jet mode through the drop-jet flow regimes. Further, the effect of the moving towards a steady jet flow is to enhance the average Nusselt number on the sub-cooled surface. Therefore, correlations available in literature may under-predict the heat removal rates for the drop-jet and jet flow modes.

3.2. Analytical and Numerical Study on Film-Condensation in a Plane Channel

In this study, analytical results for fully-developed and numerical results for developing flow in a plane channel with film-condensation are obtained. However, the results correspond to certain operating condition discussed below.

3.2.1. Physical Model of the Problem

Figure 9 shows the physical model, considered in the present study, corresponds to hydro-dynamically as well as thermally developing vapor-liquid stratified-flow in a plane channel; with heating from the top and cooling from the bottom wall. The figure shows that the liquid and vapor (at saturated condition) enters from the left boundary in fully-developed stratified flow condition, with vapor flowing on top of liquid.

The flow configuration along with axial variation of temperature profile and the two-phase interface is shown in Fig. 9(a), for the channel-walls subjected to different standard thermal boundary conditions; corresponds to four different cases (a)-(d) considered in the present work. Fig 9(b) shows the velocity profile along the channel length for both phases. As the interface curvature is small, the surface tension force associated with the interface is small enough so that the pressure jump across the interface can be neglected, and both the phases can be assumed to remain at equilibrium. As the phase change takes place from the interface, the interface is assumed to remain at saturation temperature (T_{sat}).

The thermal BCs are applied in such a manner that there is always superheating from the top wall ($T_{w2} > T_{sat}$) and sub cooling from the bottom wall ($T_{w1} < T_{sat}$). Up to a certain length in the channel there exists a difference in the wall heat flux between the top and the bottom wall ($q_{w1} \neq q_{w2}$), which leads to a jump in the heat flux across the interface and generates an interfacial mass flux from the Stephan's condition as given in Gada and Sharma (2009).

The region up to which the interface height changes, the phase change occurs along with change in thermal and velocity profile; termed as hydro dynamically and thermally developing region. Beyond this region the heat flux from the channel walls are equal in magnitude ($q_{w1} = q_{w2}$), such that there is no heat jump across the interface. This leads to no interfacial mass flux such that the velocity and the temperature profile do not change along the axial length. This region is called as fully developed (FD) region

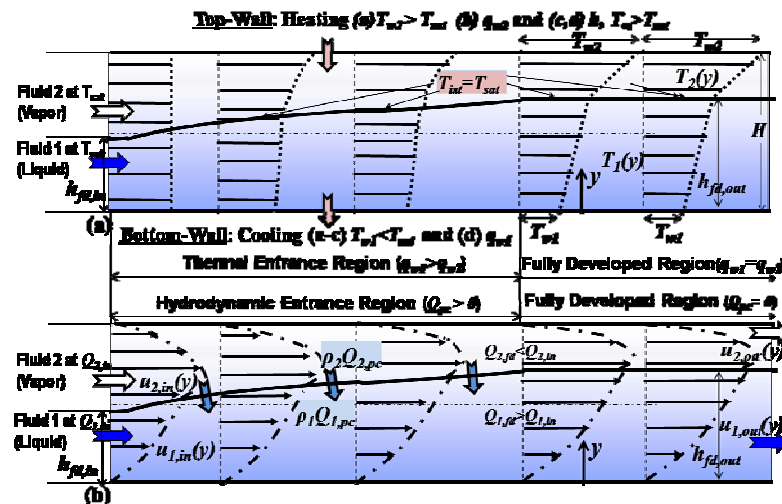


Figure 9: Physical model for (a) thermally and (b) hydro-dynamically developing flow in a plane channel, with phase-change in the developing region. Developing (a) temperature and (b) velocity profile are shown in the figure. Arrows on channel-wall in Fig. (a) represents direction of heat-flux and at the interface in Fig. (b) represents direction of interfacial mass flow rate.

3.2.2. Operating and Boundary Conditions

The analytical solution for a condensation problem proposed here corresponds to the fully developed region, such that the interface height does not change along the axial length. Note that it corresponds to phase change in the developing region with no heat transfer in the fully developed region, as the heat gained from the top becomes equal to that lost from the bottom wall of the channel. The thermo-physical properties and boundary conditions are chosen such that complete condensation of vapor to liquid does not occur.

These leads to certain operating conditions, given as

$$\frac{\partial u_1}{\partial x} = \frac{\partial u_2}{\partial x} = 0, \quad v_1 = v_2 = 0, \quad \frac{\partial H_{fd}}{\partial x} = 0 \text{ and}$$

$$\frac{\partial T_{w1}}{\partial x} = \frac{\partial T_2}{\partial x} = \frac{\partial T_{m1}}{\partial x} = 0, \quad \frac{\partial T_{w2}}{\partial x} = \frac{\partial T_2}{\partial x} = \frac{\partial T_{m2}}{\partial x} = 0 \dots\dots\dots(11)$$

The analytical solutions are proposed here for the four different types of thermal boundary conditions, given in Table 2.

Table 2: Four different cases corresponding to various thermal boundary conditions (CWT: constant wall temperature; UHF: uniform heat flux; and CHT: convection heat transfer) on the channel walls.

Cases	(a)	(b)	(c)	(d)
Top wall BC	CWT: $T_{w2} > T_{sat}$	UHF: q_w	CHT: $h \ \& \ T_{\infty} > T_{sat}$	CHT
Bottom Wall BC	CWT: $T_{w1} < T_{sat}$	CWT: $T_{w1} < T_{sat}$	CWT: $T_{w1} < T_{sat}$	UHF: q_w

3.2.3. Analytical Solution from Energy Equation

For the operating conditions proposed above, the axial and transverse advection term in the energy equation are eliminated as $\frac{\partial T_2}{\partial x} = \frac{\partial T_1}{\partial x} = 0$ and $v = 0$ respectively. Thus, for each phase, the steady state equation reduces to a 1-D steady state heat conduction equation:

$$k_f \frac{\partial^2 T_f}{\partial y^2} = 0 \dots\dots\dots(12)$$

where $f = 1$ and 2 corresponds to liquid and vapor phases respectively,

Boundary conditions at the interface are taken as

$$T_f = T_{sat} \text{ at } y = h_{fd}, \dots\dots\dots(13)$$

$$k_1 \frac{\partial T_1}{\partial y} = k_2 \frac{\partial T_2}{\partial y} \text{ at the interface } \dots\dots\dots(14)$$

Integrating Eq. (12) and using the boundary conditions at the walls (Table 2) and at the interface Eq. (13) & Eq. (14), the expressions for fully-developed temperature/heat-flux profile (in the two-phases) and interface-height are obtained. This is given in Table 3, for the four different cases considered in the present work.

Table 3: Analytical solution for fully-developed two-phase stratified flow, with condensation in the developing region, for four different cases.

Cases	Temperature Profiles		Interface Height
	$\Delta T_1(y)$	$\Delta T_2(y)$	h_{fd}
(a)	$\left(\frac{y}{h_{fd}} - 1\right) \Delta T_{sub,b}$	$\left(\frac{y - h_{fd}}{H - h_{fd}}\right) \Delta T_{sup,t}$	$\frac{k_1 H}{k_1 + k_2 \Delta T_t^*}$
(b)	$\left(\frac{y}{h_{fd}} - 1\right) \Delta T_{sub,b}$	$\frac{q_{wt}(y - h_{fd})}{k_2}$	$-\frac{k_1}{q_{wt}} \Delta T_{sub,b}$
(c)	$\left(\frac{y}{h_{fd}} - 1\right) \Delta T_{sub,b}$	$\frac{(y - h_{fd}) \Delta T_{sup,\infty}}{k_2 R_{th,tot}}$	$\frac{k_1 (hH + k_2)}{h(k_1 + k_2 \Delta T_\infty^*)}$
(d)	$\frac{q_{wb}(y - h_{fd})}{k_1}$	$\frac{(y - h_{fd}) \Delta T_{sup,\infty}}{k_2 R_{th,tot}}$	$\frac{q_{wb}(hH + k_2) + k_2 h \Delta T_{sup,\infty}}{h q_{wb}}$

In the above table, $T_1(y) = \Delta T_1(y) + T_{sat}$, $T_2(y) = \Delta T_2(y) + T_{sat}$, $\Delta T_{sub,b} = T_{sat} - T_{w1}$

$$\Delta T_{sup,t} = T_{w2} - T_{sat}, \quad \Delta T_{sup,\infty} = T_\infty - T_{sat}, \quad \Delta T_t^* = \frac{\Delta T_{sup,t}}{\Delta T_{sub,b}}, \quad \Delta T_\infty^* = \frac{\Delta T_{sup,\infty}}{\Delta T_{sub,b}},$$

$$R_{th,conv} = 1/h, \quad R_{th,cond} = (H - h_{fd})/k_2, \quad R_{th,tot} = R_{th,conv} + R_{th,cond}$$

3.2.4. Analytical Solution from Navier Stokes Equation

For the fully developed conditions and the BCs at the interface, for *isothermal* flow, Dutta et al. (2009) derived the velocity and pressure profiles from the momentum equation, This is also applicable here for the phase change, given in Table 4 in non dimensional form.

Table 4: Analytical fully developed non-dimensional velocity profile for each phases

Fluid	$U_f(Y)$
1	$A(BY - Y^2)$
2	$A(C + BY - Y^2)/\eta$

$$A = -\frac{1}{2} \frac{dP}{dX}, \quad B = \frac{1 + H_{fd}^2(\eta - 1)}{1 + H_{fd}(\eta - 1)}, \quad C = \frac{(\eta - 1)H_{fd}(1 - H_{fd})}{1 + (\eta - 1)H_{fd}}$$

$$\frac{dP}{dX} = -12Q_{1fd}^* \left[\frac{1 + H_{fd}(\eta - 1)}{H_{fd}^2[(3 - 2H_{fd} - H_{fd}^2) + \eta H_{fd}^2]} \right], \quad Q_{1fd}^* = \frac{Q_{1in}^* + \chi Q_{2in}^*}{1 + \chi Q_{r,fd}}$$

$$Q_{r,fd} = \frac{(1 - \eta)H_{fd}^4 + 2(3\eta - 2)H_{fd}^3 + 3(2 - 3\eta)H_{fd}^2 + 4(\eta - 1)H_{fd} + 1}{\eta(\eta - 1)H_{fd}^4 - 2\eta H_{fd}^3 + 3\eta H_{fd}^2}$$

$$Q_{1,in}^* = \frac{Q_{1,in}}{U_\infty H}, \quad Q_{2,in}^* = \frac{Q_{2,in}}{U_\infty H}, \quad \eta = \frac{\mu_2}{\mu_1}, \quad P = \frac{pH}{\mu_1 U_\infty}, \quad H_{fd} = \frac{h_{fd}}{H}$$

$$U_f(Y) = \frac{u_f(Y)}{U_\infty}, \quad X = \frac{x}{H}, \quad Y = \frac{y}{H}, \quad \chi = \frac{\rho_2}{\rho_1}$$

3.2.5. Numerical Solution

An in-house DGLSM based code, (Gada and Sharma, 2011) is used for the simulation of the stratified two phase flow condensation problem. The non-dimensional height and length of the computational domain is taken as 1 and 40, respectively. At the top and the bottom wall of the channel, no slip velocity BC are used and various thermal BC (corresponding to cases a – d, given in Table 2) are used. At the entry to the computational domain hydro dynamically fully developed boundary conditions are given (corresponding to the fluids viscosity ratio η and inlet flow rate ratio Q_r), using the analytical solution proposed by Dutta et al.(2009). The temperature of both the phases at the entry are at saturated condition. For the simulation Q_r (inlet flow rate ratio) = 1.272 is taken.

The simulation is done for steam-water system at near critical state, having the state parameters as $p_{\text{sat}} = 179$ bar , $T_{\text{sat}} = 630$ K and $h_{\text{fg}} = 781$ KJ/kg and the thermo physical properties corresponding to the system state are taken as

fluid 1 : $\rho_1 = 538.79$ kg/m³ , $c_{p1} = 12.6$ kJ/kg-K , $k_1 = 0.41$ W/m-K , $\mu_1 = 67\mu\text{N-s/m}^2$

fluid 2 : $\rho_2 = 133.33$ kg/m³ , $c_{p2} = 22.1$ kJ/kg-K , $k_2 = 0.13$ W/m-K , $\mu_2 = 28\mu\text{N-s/m}^2$

The inlet velocity to the computational domain is taken to be hydro dynamically fully developed, whose interface height is given by solving the non linear equation in H_{in} , given by Dutta et al. (2009), as:

$$\{\eta(\eta - 1)Q_r + \eta - 1\}H_{\text{in}}^4 + (4 - 2\eta Q_r - 6\eta)H_{\text{in}}^3 + (3\eta Q_r + 9\eta - 6)H_{\text{in}}^2 + 4\eta(1 - \eta)H_{\text{in}} - 1 = 0 \quad \dots\dots\dots(3.1)$$

Where , $\eta = \frac{\mu_2}{\mu_1}$, is the viscosity ratio, $Q_r = \frac{Q_2}{Q_1}$,

Using H_{in} in expression of $U_f(Y)$ in Table 4, the inlet velocity profile is obtained. At the exit ,the BCs are taken as fully developed. At the channel walls, the no slip and no penetration velocity conditions are used. The thermal BCs for four different cases are taken as follows:

Case (a) : $T_{w1} = 620$ K, $T_{\text{sat}} = 630$ K, $T_{w2} = 655$ K

Case (b) : $T_{w1} = 620$ K, $T_{\text{sat}} = 630$ K, $q_{w2} = -7$ W/m²

Case (c) : $T_{w1} = 620$ K, $T_{\text{sat}} = 630$ K, $T_{\infty} = 645$ K, $h = 15$ W/m²-K

Case (d) : $q_{w2} = -19$ W/m², $T_{\text{sat}} = 630$ K, $T_{\infty} = 700$ K, $h = 15$ W/m²-K

The number of grid points found sufficient for grid independent results is 800×40, with uniform grid spacing in X and Y direction as $\Delta X = 0.05$ and $\Delta Y = 0.025$, respectively.

3.2.6. Results and Discussion

The simulation is done for $Re_1 = 0.8$, at near critical points (as given before) in order to ensure lower computational time.

3.2.6.1. Fully Developed Flow

Figure 10 shows an excellent agreement between the present analytical and numerical results for temperature as well as the velocity-profile. The dashed lines in the figure show the analytically obtained fully-developed non-dimensional interface height, across which a change in slope of the profiles is seen. Furthermore, it can be seen in the figure that the numerically obtained temperature profile is linear (although the governing equations used for simulations included all the terms); corroborating our proposition that the heat transfer in fully-developed region is only due to transverse conduction.

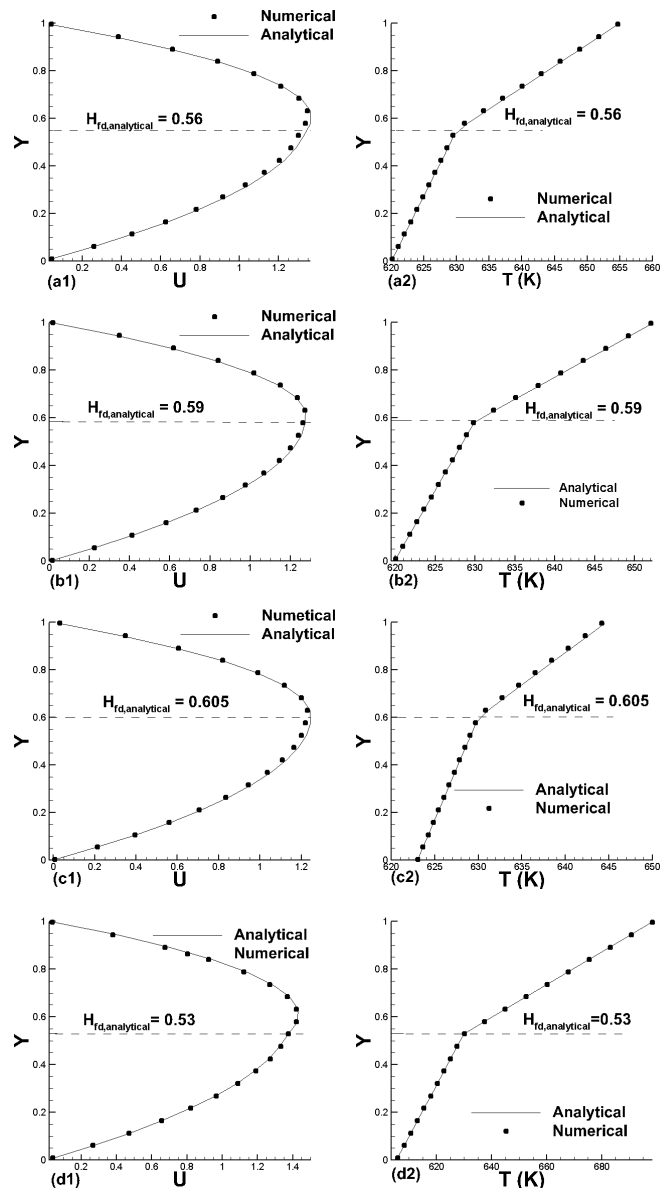


Figure 10: Fully developed (a1-d1) velocity (non-dimensional) profile and (a2-d2) temperature profile for all the four cases (a-d), along with the analytical solutions.

3.2.6.2. Developing Flow

Figure 11 shows the variation of axial velocity (non dimensional) profile and temperature profile for cases (a-d). It can be seen that the result at $X = 24$ and $X = 40$ overlaps, indicating that the flow becomes fully developed region beyond $X = 24$. Also the temperature plot shows non linear profiles near the entry (developing region) and a linear downstream (developed region). This confirms the operating condition, *i.e.*, there is no axial conduction in fully developed region. From the velocity plots (Fig. 11, (a1)-(d1)), we can see that the volumetric flow rate (*i.e.*, $\int U dY$, can be seen as area under the $U(Y)$ curve) decreases along the axial direction, indicating film-condensation along the channel length.

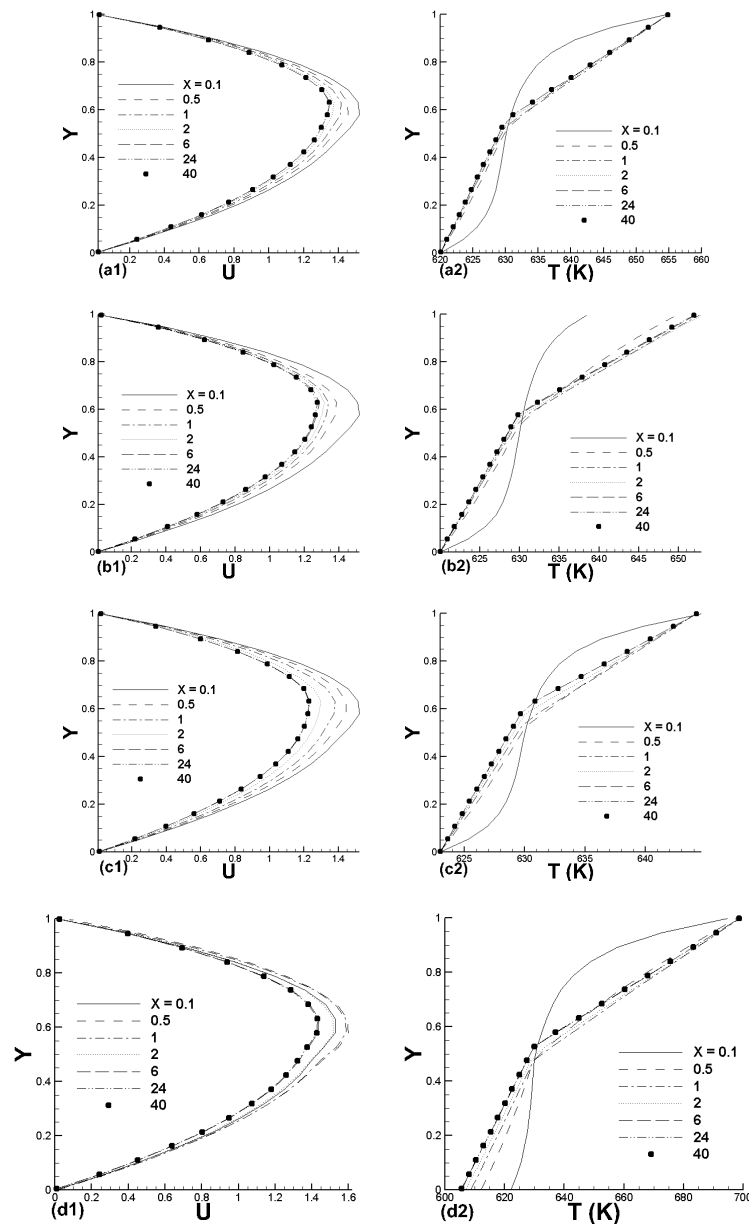


Figure 11: (a1-d1) axial velocity (non-dimensional) profile and (a2-d2) temperature profile along the channel length, for all the four cases (a-d).

Figure 12 shows the heat flux variation at both the walls with the axial length of the channel for all the cases (a-d). As the flow becomes fully developed, it is seen that the wall heat flux becomes equal ($q_{w1} = q_{w2}$), which further justifies the linear nature of the temperature profile as proposed in the operating condition.

Figure 13 shows the axial variation of U_{max} for all the cases (a – d). It is seen that U_{max} decreases along the channel length, due to condensation occurring along the channel length. It is also seen that the decrease in U_{max} is proportional to fully developed interface height (which can be correlated with H_{fd} given for all cases in other plots like Fig. 10).

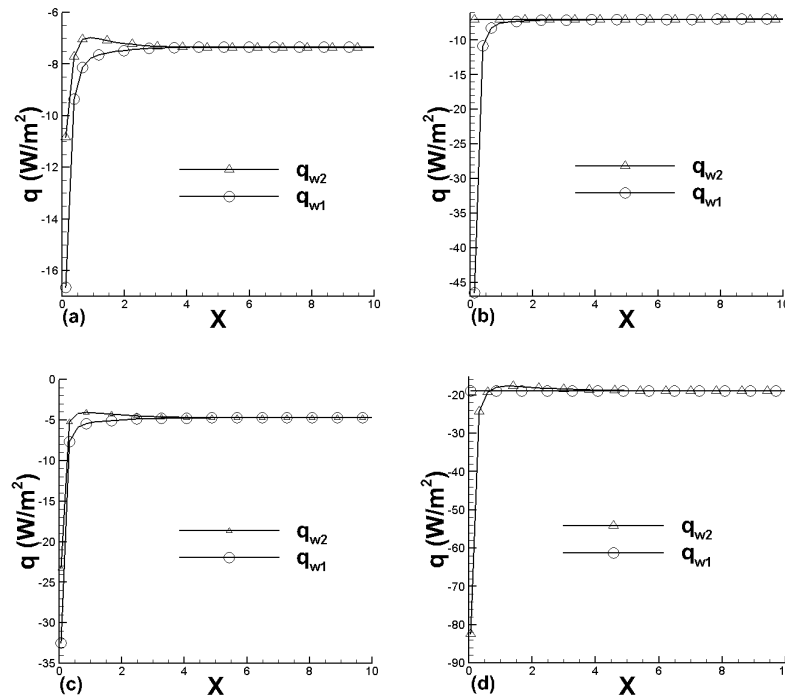


Figure 12: Axial variation of heat fluxes at the walls for the cases (a-d).

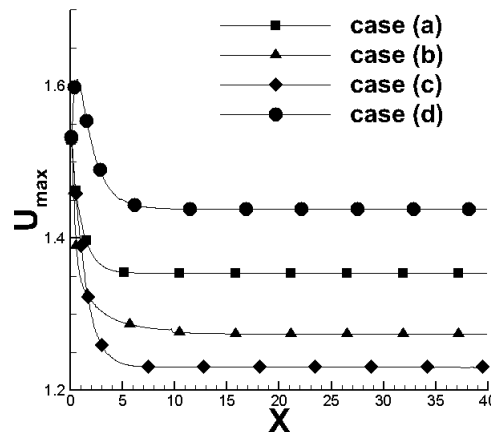


Figure 13: Axial variation of maximum velocity for the cases (a-d).

Figure 14 shows that the numerically obtained developing interface height increases along the axial length indicating a film condensation in the developing region. It asymptotes to a fully developed value, which matches very well with the analytical results. Figure 14(d) shows a slight decrease in the interface height near the inlet for the case (d), due to film-boiling followed by condensation in the downstream length.

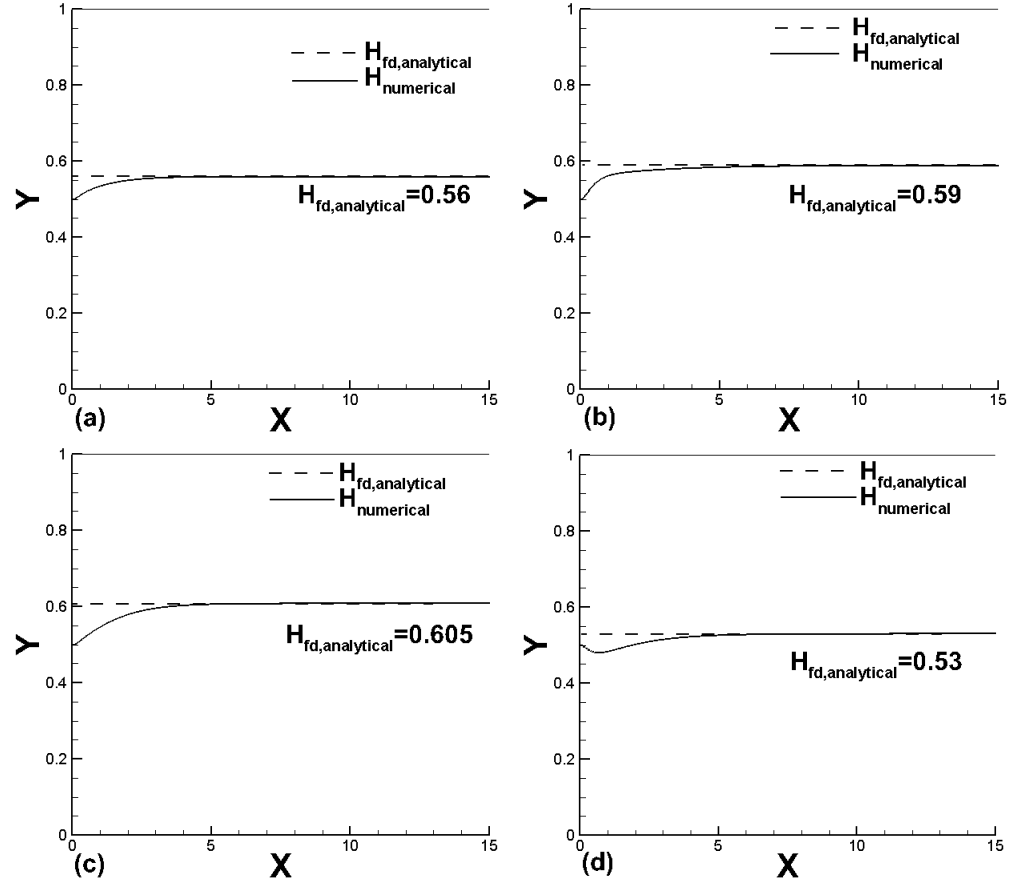


Figure 14: Numerical obtained developing interface, for all the cases (a-d). Fully developed value compared with the analytical results.

3.2.7. Conclusion

Analytical for fully-developed and numerical for developing flow is studied here, for film condensation in a plane channel. Although the flow is hydro-dynamically fully developed at the inlet, the flow redevelops due to phase change in the developing region. Thus, analytical solution of thermally (thermally and hydro-dynamically) fully-developed flow are obtained. The analytical solution is given also for non-dimensional interface-height, volumetric-flow-rate, pressure-gradient and velocity/shear-stress profile; obtained by solving Navier-Stokes as well as energy equations. Our analytical results can also be used as a test-case, for benchmarking a numerical method for two-phase flow with condensation.

Using an in-house level set method based code, 2D simulations are done for the operating conditions proposed in the analytical study. The simulations are done for four different cases, consisting of various standard thermal boundary conditions in the channel wall. For the fully-developed flow, an excellent agreement is found between the numerical

and analytical results. The numerical results obtained for the developing flow are consistent with the physical-model and operating-conditions proposed in the present work.

4. Conclusion

Out of the five technical milestones proposed in this project work (refer page no.1), the first four have been achieved and the detailed results are presented in this report.

REFERENCES

1. Alexiades, V., Solomon, A.D., 1993. Mathematical modeling of melting and freezing processes, Hemisphere Pub., Washington DC/New York, pp. 34 – 38.
2. Bellman, R., Pennington, R.H., 1954. Effects of surface tension and viscosity on Taylor Instability, Quarterly Applied Mathematics 12 151 – 162.
3. Dutta D., Gada, V.H., Sharma, A. 2011. Analytical and Level-Set Method Based Numerical Study for Two Phase Stratified Flow in a Plain Channel and a Square Duct. Numerical Heat Transfer, part A: Applications 60(4) 347-380.
4. Dhir, V.K., Taghavi-Tafreshi K., 1981. Hydrodynamic transition during dripping of a liquid from underside of a horizontal tube, ASME Winter Meeting, Washington D.C.
5. Gada, V.H., Sharma, A., 2009. On derivation and physical interpretation of level set method-based equations for two-phase flow simulations, Numerical Heat Transfer, Part B: Fundamentals 56 (4) 307 – 322.
6. Gada, V.H., Sharma, A., 2011. On a novel dual-grid level-set method for two-phase flow simulation, Numerical Heat Transfer, Part B: Fundamentals 59 (1) 26 – 57.
7. Gada, V.H., 2012. A Novel Level Set based CFMD Methodology in 2-D/3-D Cartesian and Cylindrical Coordinates and its Application for Analysis of Stratified-Flow and Film-Boiling, PhD. Thesis, Indian Institute of Technology, Bombay, INDIA.
8. Gerstmann, J., Griffith, P., 1967. Laminar film condensation on the underside of horizontal and inclined surfaces, International Journal of Heat and Mass Transfer 10 (5) 567 – 580.
9. Hu, X., Jacobi, A.M., 1996. The intertube falling film: Part 1 - Flow characteristics, mode transitions, and hysteresis, Journal of Heat Transfer 118 (3) 616–625.
10. Sharifi, P., Esmaeeli, A., 2009. Computational studies of EHD-enhanced condensation heat transfer on a downward-facing horizontal plate, IMECE2009, Florida, USA.
11. Tomar, G., Biswas, G., Sharma, A., Agrawal, A., 2005. Numerical simulation of bubble growth in film boiling using a coupled level-set and volume-of-fluid method, Physics of Fluids 17 (11) 112103.
12. Welch, S.J.W., Wilson, J., 2000. A volume of fluid based method for fluid flows with phase change, Journal of computational physics 160 (2) 662 – 882.